Spent Nuclear Fuel Vibration Integrity Study – 16332

Jy-An Wang *, Hong Wang *, Hao Jiang *, Yong Yan *, Bruce Bevard *
* Oak Ridge National Laboratory

ABSTRACT

The objective of this research is to collect dynamic experimental data on spent nuclear fuel (SNF) under simulated transportation environments using the Cyclic Integrated Reversible-Bending Fatigue Tester (CIRFT), the hot-cell testing technology developed at Oak Ridge National Laboratory (ORNL). The collected CIRFT data will be utilized to support ongoing spent fuel modeling activities, and support SNF transportation related licensing issues. Recent testing to understand the effects of hydride reorientation on SNF vibration integrity is also being evaluated.

CIRFT results have provided insight into the fuel/clad system response to transportation related loads. The major findings of CIRFT on the HBU SNF are as follows:

- SNF system interface bonding plays an important role in SNF vibration performance,
- Fuel structure contributes to the SNF system stiffness,
- There are significant variations in stress and curvature of SNF systems during vibration cycles resulting from segment pellets and clad interaction, and
- SNF failure initiates at the pellet-pellet interface region and appears to be spontaneous.

Because of the non-homogeneous composite structure of the SNF system, finite element analyses (FEA) are needed to translate the global moment-curvature measurement into local stress-strain profiles. The detailed mechanisms of the pellet-pellet and pellet-clad interactions and the stress concentration effects at the pellet-pellet interface cannot be readily obtained directly from a CIRFT system measurement. Therefore, detailed FEA is used to understand the global test response, and that data will also be presented.

INTRODUCTION

High burn-up spent nuclear fuel (SNF) cladding has a significant amount of microcracks and hydrides, which will reduce the stress intensity required for crack growth. The potential linking of microcracks during vibration loading could also reduce the fatigue threshold/incubation period significantly, accelerating fatigue failure. In addition to cladding damage, the microstructure of fuel pellets and the characteristics of the interfaces between fuel pellets and between fuel pellets and cladding are likely to be dramatically changed after high burn-up. These modifications can have a direct impact on the structural integrity and vibration response of SNF rods in transportation.

As a result, vibration has been included as one of the mandatory testing conditions in the structural evaluation of packages used by the US Nuclear Regulation Commission (NRC) in transporting SNF (10 CFR §71.71). Prior to this program development, no current system was available to test the SNF and evaluate the performance of fuel rods during spent fuel transportation. The objective of this research is to develop a system that can appropriately test the response of high-burnup SNF rods in a simulated loading condition.

Also, the predominance of the hydride platelets that do exist in the cladding after the fuel being discharged from reactors is oriented in the circumferential direction. At elevated temperatures during drying-transfer, some of the hydrogen may go into solution (up to 200 wppm at 400°C). The pressure-induced cladding tensile hoop stress during drying-transfer operations is high relative to in-reactor and pool-storage conditions. During cooling under tensile hoop stress, some of the dissolved hydrogen will precipitate in the radial direction across the cladding wall. Further cooling during storage may result in radial-hydride-induced embrittlement.

The objective of this project is to collect experimental data on spent nuclear fuel (SNF) from pressurized water reactors (PWRs), including H. B. Robinson (HBR) and North Anna (NA) Zircaloy-4 cladding and NA and Catawba M5 cladding, and the Limerick Generating Station boiling water reactor (BWR) under simulated transportation environments using the Cyclic Integrated Reversible-Bending Fatigue Tester (CIRFT), an enabling hot-cell testing technology developed at Oak Ridge National Laboratory [1-5] (ORNL). This data will be used to support ongoing spent fuel modeling activities, in addition to addressing licensing issues associated with SNF transport.

Testing on SNF rods from PWRs—HBR and NA Zircaloy-4 cladding and Catawba M5 cladding [6-8]—demonstrated that the cyclic fatigue lifetime of SNF rods generally depends on the amplitude of applied moment when a 5 Hz waveform is used. It was also demonstrated that the lifetime of SNF is related to the degree of damage to cladding and fuel pellets resulting from irradiation after a long term of service inside a reactor, as well as the loading amplitude and loading rate of applied moment, due to different fatigue damage mechanisms triggered by the intensity of pellet-clad mechanical interaction. The FY15 study extends the vibration data collected to include Zircaloy-2 data from a BWR environment. An S-N trend similar to that of the PWR data was also observed in the BWR data. Detailed high-burnup (HBU) HBR CIRFT test results are published in NUREG/CR-7198 [9]. Furthermore, the accumulated damage from the combination of low-amplitude CIRFT cyclic bending plus transient shocks (high-amplitude bending load) indicates an accelerated aging effect compared to that of low-amplitude cyclic bend loading alone.

CIRFT TESTING ON BWR LIMERICK SNF RODS

In FY 2015, 14 SNF rod segments from the Limerick (LMK) boiling water reactor (BWR) were tested using the ORNL CIRFT equipment—one test under static conditions and 13 tests under dynamic loading conditions. Under static unidirectional loading, a moment of 85 N·m was obtained at a maximum curvature of 4.0 m^{-1}. The specimen did not show any sign of failure during three repeated loading cycles to a similar maximum curvature. Thirteen cyclic tests were conducted with load amplitudes varying from 25.4 to 7.1 N·m. Failure was observed in 12 of the tested rod specimens. The cycles-to-failure ranged from 2.14×10^4 to 4.70×10^6. One cycled to 7.58×10^6 without failure, and the test was stopped. The measurements taken once the test was stopped indicated a range of flexural rigidity from 30 to 50 $N \cdot m^2$. The online monitoring revealed that the flexural rigidity was slightly lower due to the higher loading, from 25 to 42 $N \cdot m^2$. This level of rigidity was a little lower than that of the PWR HBR specimens at 39 to 51 $N \cdot m^2$. While the two claddings were based on Zircaloy-2 and Zircaloy-4, respectively, it is interesting to note that the geometrical sizes contribute more to the observed difference, where HBR rods had a relative smaller cladding outer diameter (OD) and pellet diameters compared to those of the Limerick BWR. Thus, the observed higher rigidity of HBR pressurized water reactor (PWR) SNF may primarily be due to the higher strength of Zircaloy-4 cladding and higher pellet-clad interface bonding of the PWR pressurized environment. A BWR has about half the coolant pressure of a PWR.

In general, no substantial change of rigidity was observed based on the online monitoring during the cyclic fatigue testing process. Overall, the decreasing trend in lifetime with the increasing load amplitude is well defined.

The LMK03 CIRFT test results are illustrated below to demonstrate typical LMK dynamic performance..

CIRFT Test on LMK03/575B-A, ±10.16 N·m, 5 Hz

The test on LMK03/575B-A was conducted at ± 10.16 N·m, 5 Hz. The applied moment was higher than that of LMK02, and the lifetime of the specimen was accordingly longer at 4.92×10^5 cycles.

Periodic quasistatic measurements of rod deformation were conducted using two relative displacement levels (0.2 and 0.4 mm) at the selected target number of cycles. The variations in curvature range, moment range, and flexural rigidity as a function of number of cycles are given in Fig. 1. The rigidity of the measurements at the two displacements started with 44 to 48 $N \cdot m^2$, dropped to less than 40 $N \cdot m^2$ around 10^3 cycles, and remained nearly at a constant level afterwards.

The curvature, moment, and flexural rigidity based on online monitoring data are presented in Fig. 2. The online monitoring showed a flexural rigidity of about 35 $N \cdot m^2$, a little lower than that observed in measurements. Again, an abrupt decrease in flexural rigidity was seen before the final failure.

The failure occurred in the gage section again as shown in Fig. 3. The failed specimen was manually broken into two pieces for fractographic study. The images of lateral surface and fracture surfaces are presented in Fig. 4. Again, the fracture occurred on the pellet-to-pellet interface. Cracks developed in pellets, and pellets fractured into several large size fragments that were held in place. No apparent gap can be seen between the pellet and cladding. On the specimen ID side, a gray area can be seen. At this magnification level, it cannot be determined if the gray area is a damage area.

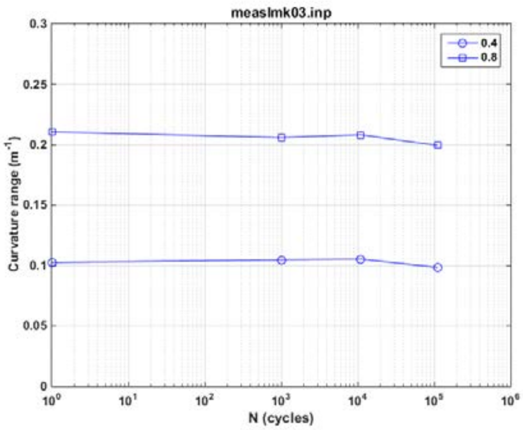

(a)

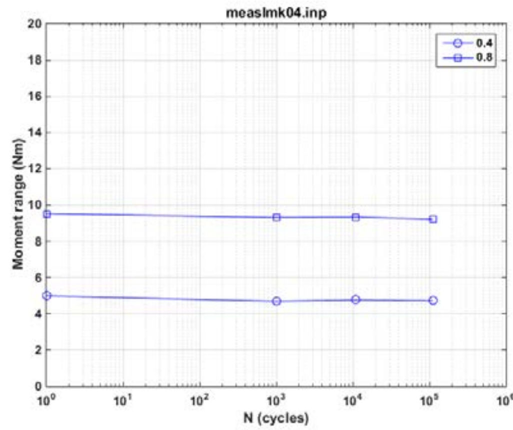

(b)

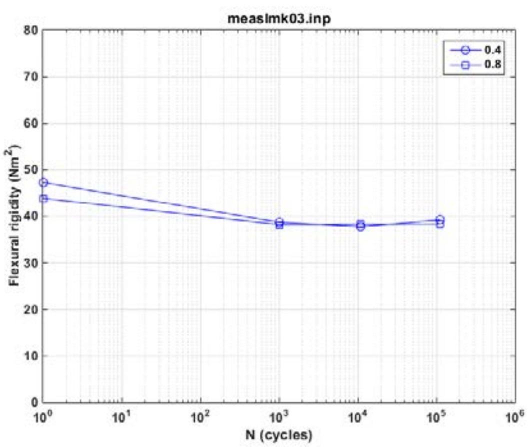

(c)

Fig. 1. Variations in (a) curvature range, (b) moment range, and (c) flexural rigidity as a function of the number of cycles for LMK03/575B-A; N_f = 4.92 × 10^5 cycles at ±10.16 N·m, 5 Hz.

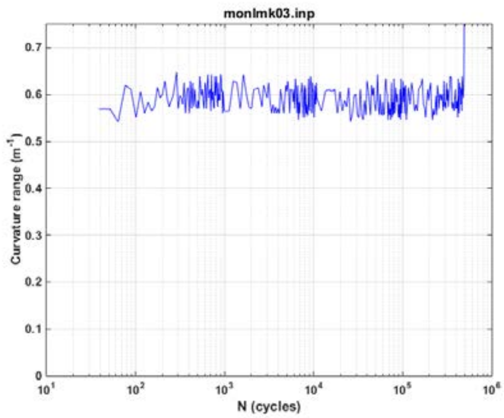

(a)

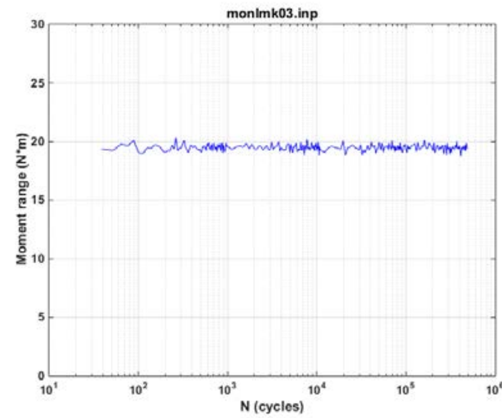

(b)

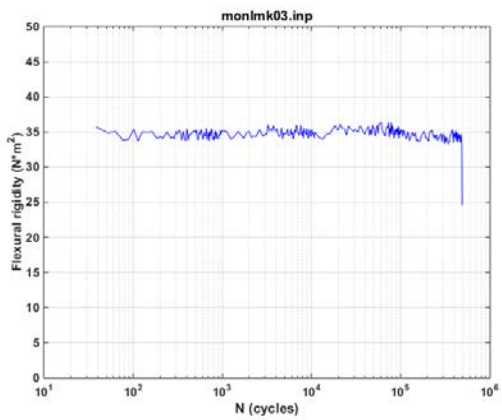

(c)

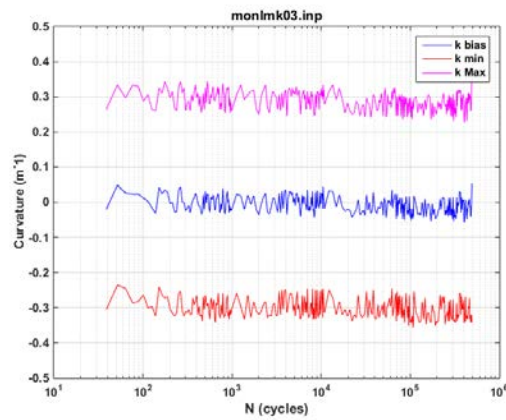

(d)

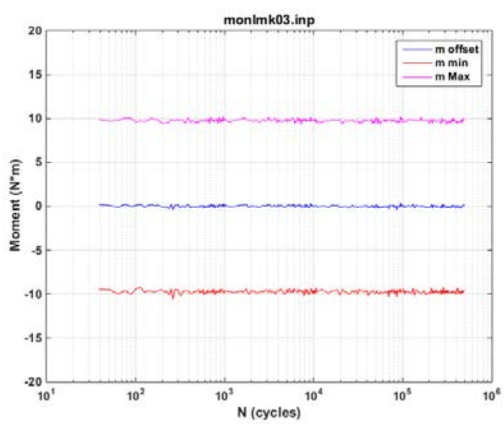

(e)

Fig. 2. Variations in (a) curvature range, (b) applied moment range, (c) flexural rigidity, (d) maximum and minimum values of curvature, and (e)

maximum and minimum values of moment as a function of the number of cycles for LMK03/575B-A; N_f = 4.92 × 10^5 cycles at ±10.16 N·m, 5 Hz.

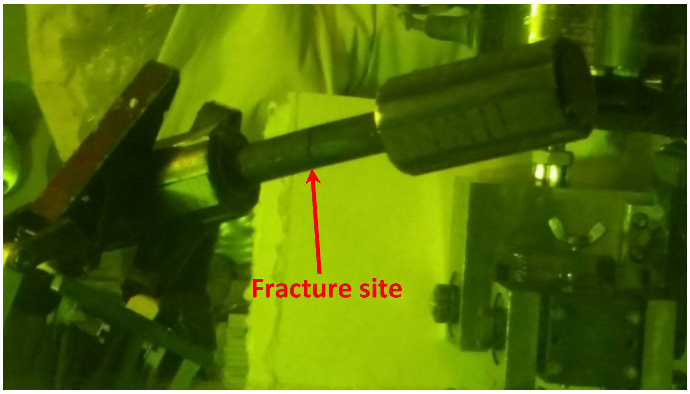

Fig. 3. Fracture segments for LMK03/575B-A N_f = 4.92 × 10^5 cycles at ±10.16 N·m, 5 Hz.

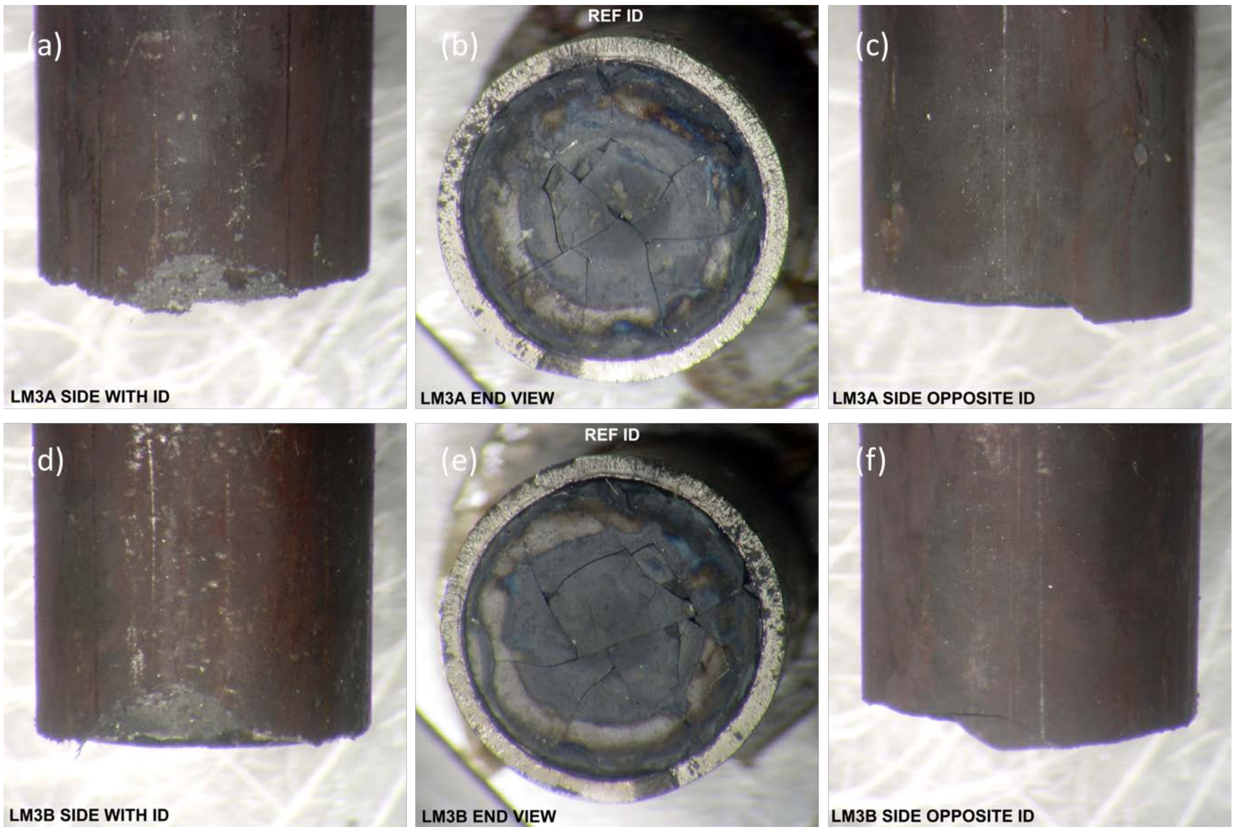

Fig. 4. Fracture segments for LMK03/575B-A. (a) and (d) show the specimen ID side of the segment on end caps A and B; (b) and (e) show the mating fracture surface; and (c) and (f) show the opposite specimen ID side of the segment on end caps A and B.

NA SNF Rod CIRFT Testing

Additional CIRFT tests were performed on three North Anna (NA) spent fuel rods and six mixed oxide (MOX) rods in a hot cell in FY15. A total of six dynamic tests were completed on NA rods in the hot cell. Applied moment amplitudes were varied from ±5.08 to ±15.24 N·m. Five specimens failed with fatigue lives ranging from 1.26×10^4 to 4.27×10^5 cycles. One specimen cycled to 5.11×10^6 without failure. Ten dynamic tests were also conducted on MOX spent fuel rods with amplitudes ranging from 5.08 to 15.24 N·m, and the specimens failed between 1.29×10^4 and 2.15×10^6 cycles. Online monitoring indicated a variation in rigidity of 21 to 28 N·m^2 for this group of spent fuel rods that had a similar cladding OD. Apparently, the range of flexural rigidity is much lower than that of HBR and LMK rods mainly due to the smaller size cross section of the rods.

The use of equivalent strain and equivalent stress obviously reduced the cladding/pellet size effect to a certain extent, and data points can be consolidated more to the HBR curve. More investigation is required to understand the performance of SNF fatigue life in terms of these quantities, including cladding materials, pellets, cladding-to-pellet and pellet-to-pellet interface bonding, and cladding oxide and hydrides.

INTERFACE BONDING EFFICIENCY STUDY FOR BWR AND PWR SNF RODS

Due to the inhomogeneous composite structure of the SNF system, finite-element analyses (FEAs) are needed to translate the global moment-curvature measurement into local stress-strain profiles for further investigation. Furthermore, the detailed mechanisms of the pellet-pellet and pellet-clad interactions and the stress concentration effects at the pellet-pellet interface cannot be readily obtained from a CIRFT system measurement. Therefore, detailed FEAs will be necessary for further interpretation of the global test response.

The FEA simulation focused on the BWR fuel rods and the results were compared with that of the PWR HBR fuel rods, which were validated and benchmarked using data from CIRFT. This report provides analysis and conclusions concerning the pellet-pellet and pellet-clad interactions of SNF vibration performance, including (1) the distribution of moment-carrying capacity between pellets and clad and (2) the impact of clad material on the flexural rigidity of the fuel rod system. The immediate consequences of interface debonding are a shift in the load-carrying capacity from the fuel pellets to the clad and a reduction in the flexural rigidity of the composite rod system. Therefore, the flexural rigidity of the fuel rod and the bending moment resistance capacity between the clad and fuel pellets are highly dependent on the interface bonding efficiency at the pellet-pellet and pellet-clad interfaces. Furthermore, the curvature and associated flexural rigidity estimates based on tests conducted on the CIRFT system are very different from the localized clad data at the pellet-pellet interface region as estimated by FEA, where the local tensile clad curvature is approximately three to four times that of the global curvature at the tension side of the clad.

The initial comparison of bending flexural rigidity variation at different bonding efficiencies between PWR and BWR is summarized below.

Flexural rigidity comparison of LMK BWR Zircaloy-2 clad and PWR HBR Zircaloy-4 clad

Interface bonding conditions	**BWR flexural rigidity EI ($N{\cdot}m^2$)**	**PWR HBR flexural rigidity EI ($N{\cdot}m^2$)**	**Difference from BWR to PWR HBR (%)**
Perfect bond	99	77	22
Pellet-pellet interface with gap debond, pellet-clad interface bonded	76	39	49
Pellet-pellet interface with gap debond, pellet-clad interface debonded	35	29	17
Pellet-pellet interface without gap debond, pellet-clad interface bonded	84	53	37
Pellet-pellet interface without gap debond, pellet-clad interface debonded	54	43	20

CIRFT test results indicate that the FEA-simulated BWR flexural rigidity was significantly overestimated, for perfect bond or partial debonding cases. This is because of the original UO_2 fuel property used in the BWR FEA study as well as the assumption made regarding the similar interface bonding efficiency between BWR and PWR environments. However, post-irradiation investigation (PIE) indicates that the BWR fuel pellet has more fracture intensity than that of the PWR fuel pellet; furthermore, PWR SNF should have a higher interface bonding efficiency than that of BWR fuel due to higher radial compressive residual stress induced by higher coolant pressure. Thus, the combined effect of BWR-degraded spent fuel and interface bonding deficiency was taken into consideration in follow-on FEA simulations by reducing the Young’s modulus to 25% and 50% to quantify the interface bonding conditions that result in similar estimated rigidity to CIRFT SNF testing results, at pellet-pellet interface debond and pellet-clad interface bond conditions. The final BWR rod FEA simulation results are shown below, which indicate that updated FEA results, with consideration given to fuel module reductions, are more appropriate and consistent with those of CIRFT test results.

Flexural rigidity comparison of BWR Zr-2 clad with fuel properties reduction consideration

Interface bonding conditions	**Fuel UO_2 full E Flexural rigidity, EI ($N \cdot m^2$)**	**Fuel UO_2 ½ E Flexural rigidity, EI ($N \cdot m^2$)**	**Fuel UO_2 ¼ E Flexural rigidity, EI ($N \cdot m^2$)**
Perfect bond	99	68	52
Pellet-pellet interface with gap debond, pellet-clad interface bonded	76	57	47
Pellet-pellet interface with gap debond, pellet-clad interface debonded	35	35	35
Pellet-pellet interface without gap debond, pellet-clad interface bonded	84	62	49
Pellet-pellet interface without gap debond, pellet-clad interface debonded	54	47	42

OUT OF CELL HYDRIDE REORIENTATION EXPERIMENTS

The objective of this hydride reorientation study is to collect experimental data on the hydride reorientation testing of HBR high burnup fuels under simulated conditions of SNF drying operations. This paper describes a procedure and test results of out-of-cell hydride reorientation tests of hydrided HBR cladding, which will be used as a guideline of in-cell hydride reorientation tests with high burnup fuel segments.

Out-of Cell Hydride Reorientation Tests at 400°C

The reorientation system consists of a high pressure piping system and test chamber within a programmable crucible furnace (see Fig. 5). For each experiment, a six-inch-long specimen, (welded with two end plugs with

Fig. 5 Hydride reorientation system.

one end sealed and the other opened) was connected to the high pressure piping system within the test chamber. The test chamber was purged with pure argon gas, and then the sample was internally pressurized to cause a hoop stress ranging from zero to 150 MP **Error! Bookmark not defined.**. Pressurized samples were subjected to a preprogrammed temperature profile for up to five cycles with each cycle being heated to 400°C, held for 2 hours, and slow-cooled/heated (1°C/min.) to 170°C with the final cycle cooled from 170°C to room temperature (RT). Hoop stress was calculated using values r = 4.62 mm for inner radius and t = 0.76 mm for the wall thickness of the HBR Zircaloy-4 cladding. The above procedure was performed in an out-of cell environment; where several reorientation tests were carried out to optimize test parameters. And the results show that multiple thermal cycles can provide more radial hydrides, as shown in Fig. 6.

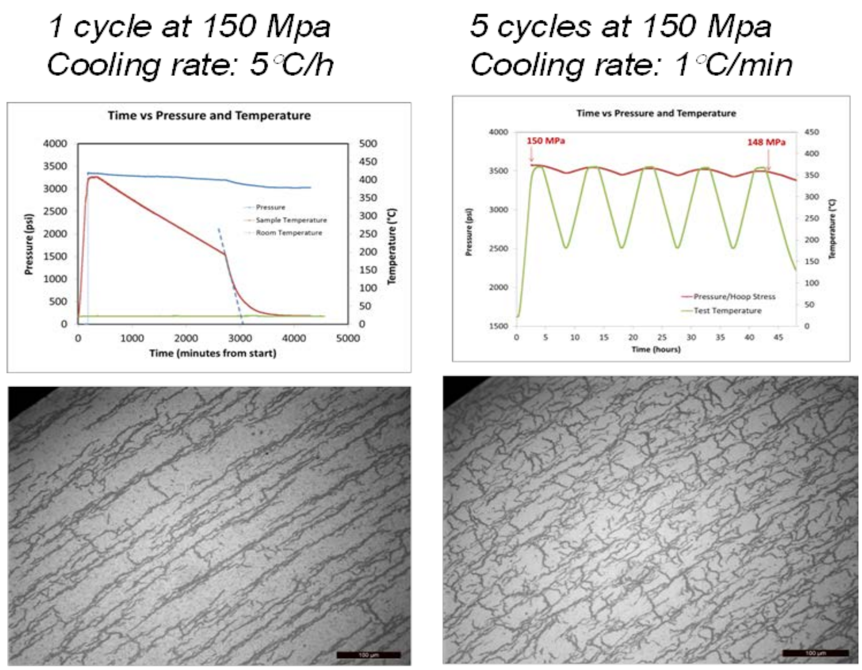

Fig. 6 Out-of cell hydride reorientation experiments.

DISCUSSION

CIRFT Moment-Curvature Curves and SNF Fatigue Strength

The fatigue curves of Limerick rods were compared with those of HBR, NA, and MOX fuels in terms of amplitude of moment and strain, and results are given in Figs. 7 and 8. The strain amplitudes were obtained according to Eq. (1).

$\varepsilon = \kappa \times y_{max}$. (where, κ is curvature and y_{max} is the radius of the cladding.) (1)

The data points for NA and MOX fuels are generally below the curve of moment amplitude versus N_f (cycles-to-failure, M-N curve) of HBR fuel, mainly due to the smaller cladding diameters of these fuels. Using strain amplitudes as a function of cycles will filter out some variability in SNF's dimensions and makes the data points from NA and MOX come close to M-N curve of HBR rods. Furthermore, due to the relatively lower rigidity of LMK compared to that of HBR, the LMK strain amplitude profile appeared to be above the HBR trend curve.

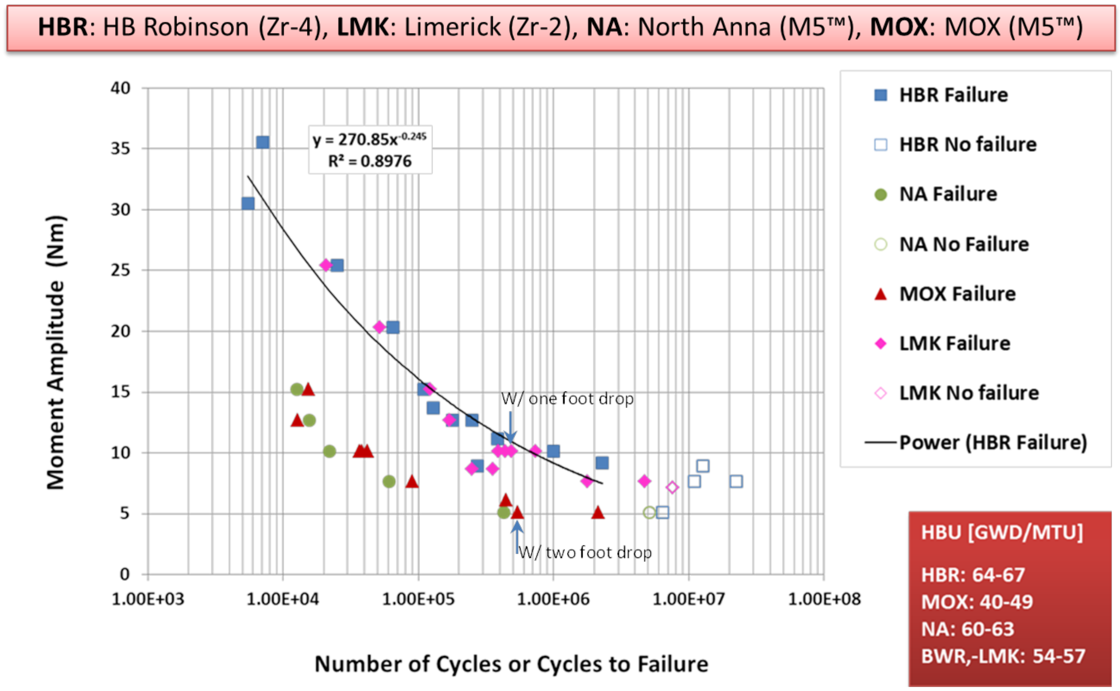

Fig. 7 Moment amplitudes as a function of number of cycles; results are based on CIRFT testing of various used fuels at 5 Hz. The power function was obtained from curve fitting based on the HBR data set. CIRFT fatigue test results reveal data scatter due to different types/sizes and burnup of clads tested.

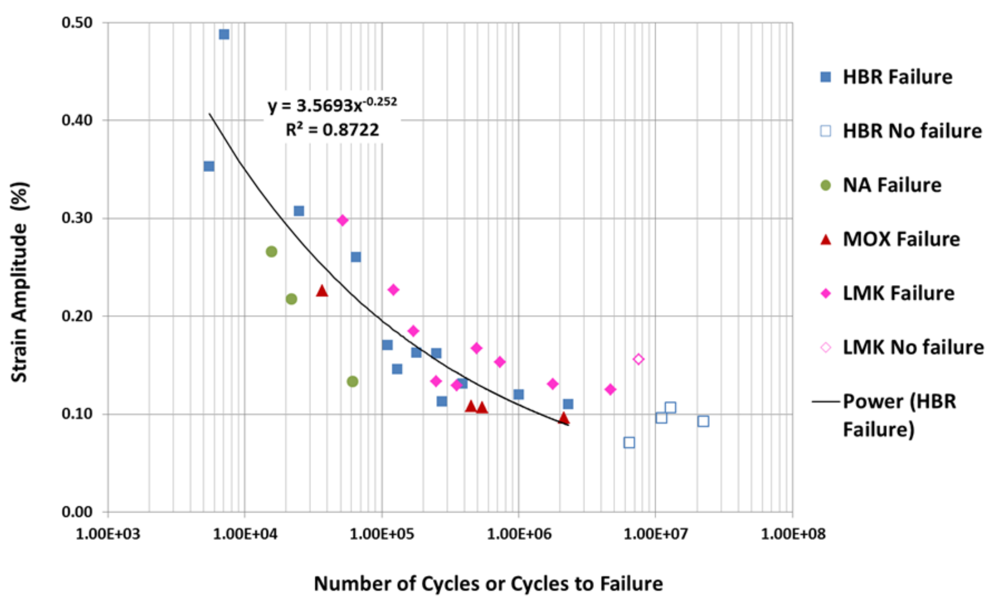

Fig. 8 Strain amplitudes as a function of number of cycles; results are based on CIRFT testing of various used fuels at 5 Hz. The power function was obtained from curve fitting based on the HBR data set.

In order to further quantify or estimate the damage potential of the transient shock to the SNF vibration lifetime, a pilot study was carried out on MOX and LMK SNF. The CIRFT specimens were dropped two to three times from heights ranging from 1 to 2 ft to simulate the transient shock prior to initiating the CIRFT bending cycling test at a frequency of 5 Hz. The accelerated aging effects of the tested MOX and LMK CIRFT samples that had been dropped are shown in Fig. 7, marked with blue arrows. The LMK CIRFT rods that were dropped 1 ft at 10 N-m load show a 50% reduction in fatigue life. MOX CIRFT rods that were dropped 2 ft at 5 N-m load show a 73% reduction in fatigue life. Noted that one MOX rod at a 10 N-m loading level that had been dropped 2 ft does not show any accelerated aging. Due to variability of SNF rods and their inherent defect intensity, a more controlled CIRFT testing protocol needs to be included in the follow-on CIRFT high-rate testing program development.

CONCLUSION

CIFRT test data provide new insights into SNF dynamic behavior. The CIRFT approach also successfully demonstrates the controllable fatigue fracture on HBU SNF in a normal vibration mode, which enables us to examine the underlying mechanism of SNF system dynamic performance. Lessons learned from CIRFT testing on SNF vibration integrity are summarized as follows.

- Fuel contribution to clad stiffness during random vibration
- Stress concentration effects on clad at pellet-pellet interfaces
- Relationship of flexural deformation mechanism to SNF rod aging history
- Potential hydrogen effects on SNF vibration integrity
- Pellet-clad bonding efficiency on SNF mechanical properties
- Finite element analysis is needed to translate CIRFT data into local stress-strain profiles
- Failure mechanisms of HBU SNF rods
- Potential impact of combined loading modes and loading rates

REFERENCES

1. J.-A. J. Wang, H. Wang, T. Cox, and Y. Yan, *Progress Letter Report on U-Frame Test Setup and Bending Fatigue Test for Vibration Integrity Study (Out-of-Cell Fatigue Testing Development–Task 2.3)*, ORNL/TM-2012/417, Oak Ridge National Laboratory, Oak Ridge, Tenn., August 2012.
2. J.-A. J. Wang, H. Wang, and T. Tan, Reversal Bending Fatigue Testing, Pub. No. US 2013/0205911 A1, Aug. 15, 2013; also as US Patent No. US 8,863,585 B2, Oct. 21, 2014.
3. H. Wang, J.-A. J. Wang, T. Tan, H. Jiang, T. S. Cox, R. L. Howard, B. B. Bevard, and M. E. Flanagan, "Development of U-frame Bending System for Studying the Vibration Integrity of Spent Nuclear Fuel," *Journal of Nuclear Materials,* **440**, 201–213 (2013).
4. J.-A. J. Wang, H. Wang, T. Cox, and C. Baldwin, *Progress Letter Report on Bending Fatigue Test System Development for Spent Nuclear Fuel Vibration Integrity Study (Out-of-Cell Fatigue Testing Development–Task 2.4)*,

ORNL/TM-2013/225, Oak Ridge National Laboratory, Oak Ridge, Tenn., July 2013.

5. J.-A. J. Wang, H. Wang, B. B. Bevard, R. L. Howard, and M. E. Flanagan, *Reversible Bending Fatigue Test System for Investigating Vibration Integrity of Spent Nuclear Fuel During Transportation*, PATRAM 2013, DOE/NRC/DOT, San Francisco, Calif., August 18–23, 2013.
6. J.-A. J. Wang and H. Wang, *The Development of Reversible Bending Fatigue Tester and Its Application to High Burn-up Spent Nuclear Fuel Integrity Study under Normal Transportation Vibration*, ORNL/TM-2013/573, August 2014. http://info.ornl.gov/sites/publications/Files/Pub47469.pdf
7. J.-A. Wang and H. Wang, *2014 Semi-Annual Progress Letter Report on Used Nuclear Fuel Integrity Study in Transportation Environments*, prepared for US Department of Energy, ORNL/TM-2014/63, April 2014. http://info.ornl.gov/sites/publications/Files/Pub48652.pdf
8. J.-A. J. Wang, H. Wang and H. Jiang, *FY14 Status Report: CIRFT Testing Results on High Burnup UNF*, ORNL/LTR-2014/310, September 2014. http://info.ornl.gov/sites/publications/Files/Pub51054.pdf
9. J.-A. Wang and H. Wang, *Mechanical Fatigue Testing of High-Burnup Fuel for Transportation Applications,* NUREG/CR-7198, ORNL/TM-2014/214, May 2015.

ACKNOWLEDGEMENTS

This research was sponsored by the DOE Used Fuel Disposition Campaign and NRC under DOE contract DE-AC05-00OR22725 with UT-Battelle, LLC. Authors thank Chuck Baldwin for PIE, Josh Schmidlin for fuel rod cutting and dimension measurement; Bryan Woody and Scot Thurman for hot-cell operation support.